Geophysical Research Letters

Supporting Information for

Dynamic rupture process of the 2023 Mw 7.8 Kahramanmaras earthquake: Variable rupture speed and implications for seismic hazard

Zijia Wang[1], Wenqiang Zhang[2], Tuncay Taymaz[3], Zhongqiu He[1], Tianhong Xu[1], Zhenguo Zhang[1,4]

[1]Department of Earth and Space Sciences, Southern University of Science and Technology, Shenzhen, China.
[2]Department of Earth and Planetary Sciences, McGill University, Montreal, Canada.
[3]Department of Geophysical Engineering, The Faculty of Mines, Istanbul Technical University, Maslak, Sarıyer, Istanbul, Türkiye.
[4]Guangdong Provincial Key Laboratory of Geophysical High-resolution Imaging Technology, Southern University of Science and Technology, Shenzhen, China

Contents of this file

Text S1, Figures S1 to S6 and Table S1.

Additional Supporting Information (Files uploaded separately)

Captions for Movies S1 to S2

Introduction

This supporting material includes supplementary figures of stress and friction parameter settings (Figure S1-S3), and a waveform comparison of several stations with incomplete records (Figure S4). In addition, text S1 and Figure S5-S6 supplement the necessity of heterogeneous of the stress orientation and friction coefficients.

Text S1. The necessity of heterogeneous of the stress orientation and friction coefficients

We present the initial shear stress and relative fault strength S of three homogeneous stress orientation case (Figure S5). It is obvious from the S value that when the stress orientation is N169° or N180°, the northeast segment of the EAF will be very difficult to rupture (S value even smaller than 0, that is, the stress drop is negative). Coincidentally, if the stress orientation is N201°, the NPF and the southwest segment of the EAF will be very difficult to rupture. Therefore, consider the clockwise trend of stress orientation is necessary.

Furthermore, we calculate the distribution of initial shear stress and S value when the friction coefficients of the EAF is uniform (Figure S6). From the S value, we can expect that there will be a sustain supershear rupture in the northeast segment of the EAF. However, in this case, the waveforms of the four stations in Figure S4 will arrive earlier, and if so, these four stations should record more waveforms before the recording stops suddenly. This is inconsistent with the observation. Therefore, we increase the friction coefficients of the easternmost segment of the EAF (see Figure S2) according to the geological survey results of Khalifa et al. (2018).

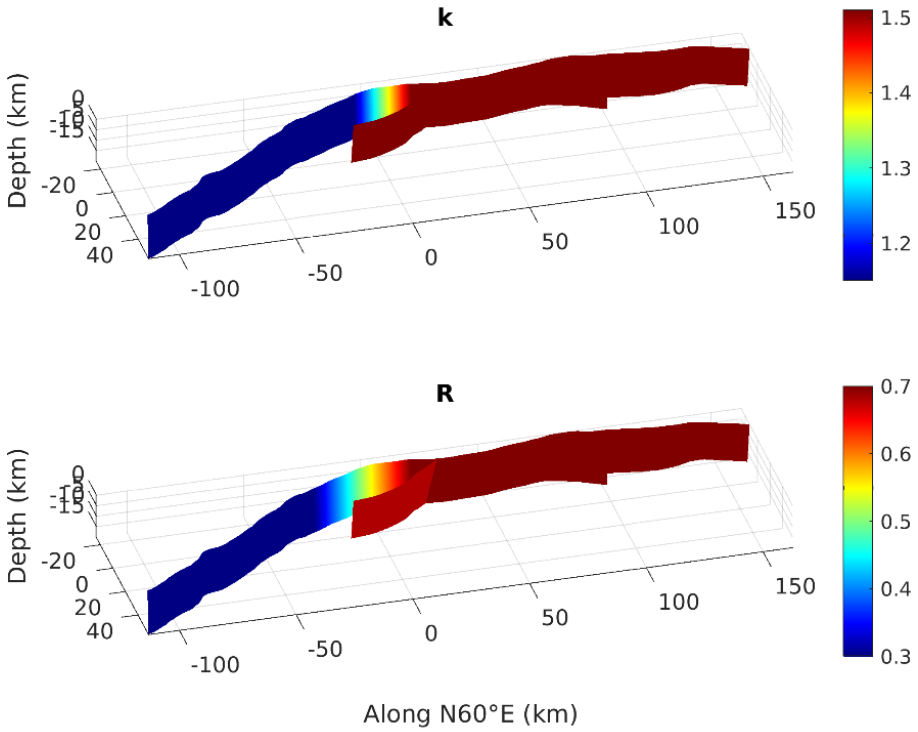

Figure S1. The distribution of lateral pressure coefficient *k* and stress shape ratio *R*. On the NPF, $k = 1.51$ and $R = 0.68$. On the southwest segment of the EAF, $k = 1.15$ and $R = 0.3$. On the F3 and the northeast segment of the EAF, $k = 1.51$ and $R = 0.7$.

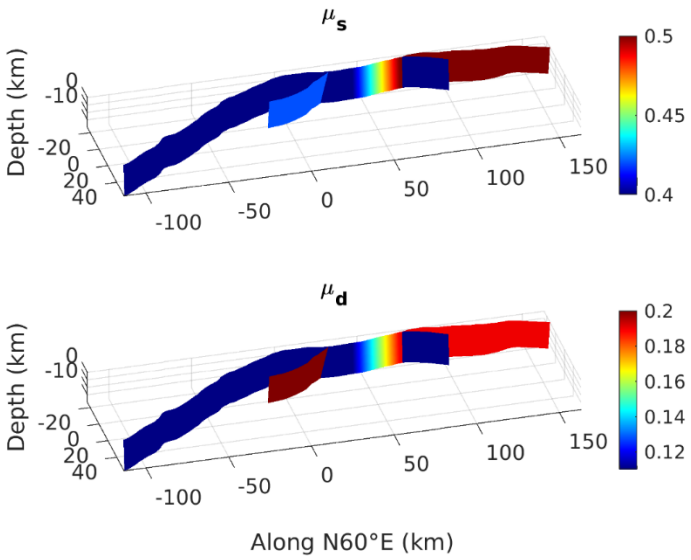

Figure S2. The distribution of static and dynamic friction coefficients μ_s and μ_d. On the NPF, $\mu_s = 0.42$ and $\mu_d = 0.2$. On the F3 and the southwest segment of the EAF, $\mu_s = 0.4$ and $\mu_d = 0.11$. On the northeast segment of the EAF, μ_s increases to 0.5 and μ_d increases to 0.19.

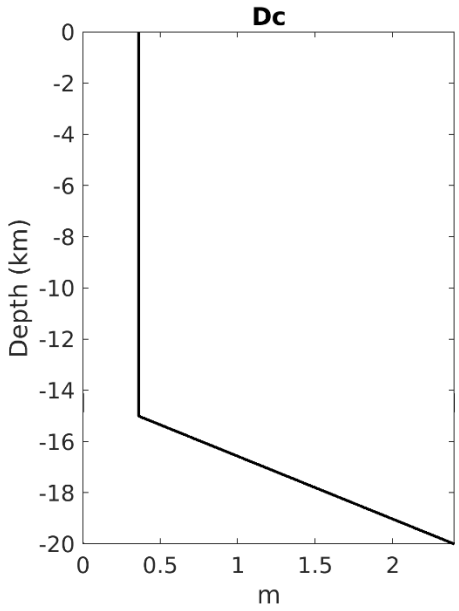

Figure S3. Variation of critical slip distance *Dc* with depth. Dc reaches a maximum of 2.4 m at a depth of 20 km.

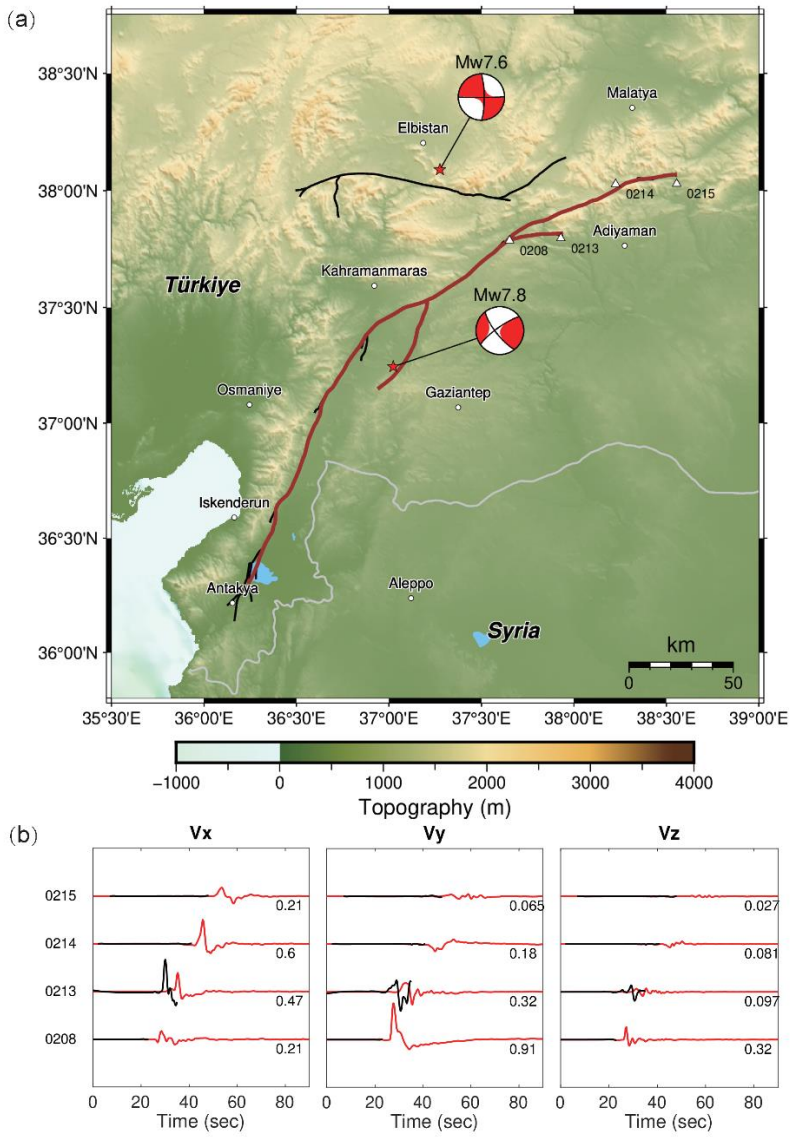

Figure S4. Comparison of incomplete waveform records of four near-fault stations in the northeast segment of EAF. (a) The location of four stations (white hollow triangle). Other things are same as Figure 1 in the text. (b) Waveform comparison. The black line is the observed waveform, and the red line is the synthesized waveform, both of which are filtered to 0.01-0.4 Hz. The station name is marked on the left. The maximum absolute values of each component of the synthesized waveform (m/s) are listed at the end of each seismogram.

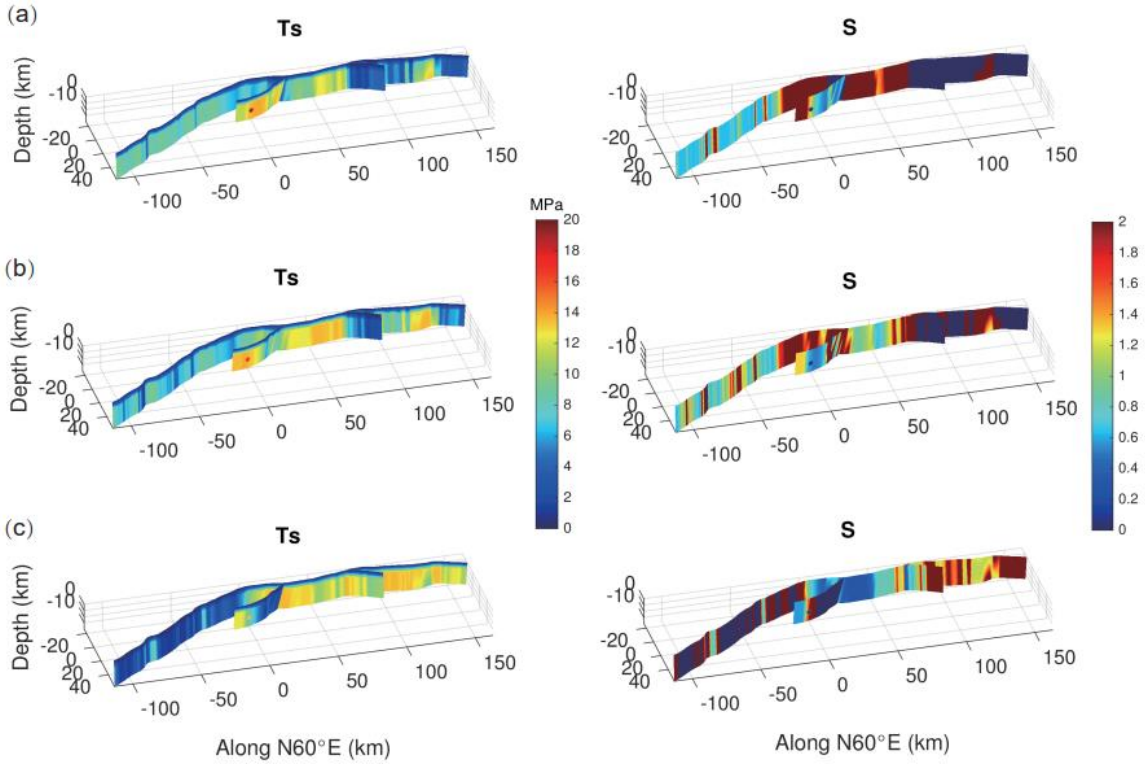

Figure S5. Initial shear stress and relative fault strength S in different homogeneous SH orientation cases. (a) SH orientation N169°E; (b) SH orientation N180°E; (c) SH orientation N201°E.

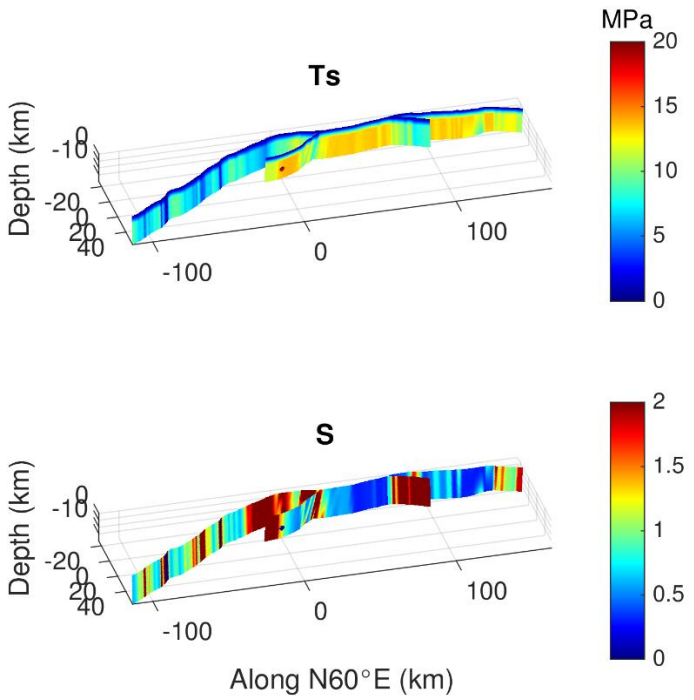

Figure S6. Initial shear stress and relative fault strength S with uniform friction coefficient of the EAF.

Tabel S1. Layer velocity model used in the dynamic simulation (Form Güvercin et al., 2022, Tabel S1)

Depth (km)	Vp(m/s)	Vs(m/s)
0	3880	2040
1	4520	2430
2	5620	3030
4	5750	3310
6	5850	3380
8	5960	3430
10	6000	3440
12	6050	3460
16	6320	3620
20	6400	3670
25	6830	3920
30	6890	3940
37	7800	4400
45	8220	4560
60	8300	4610

Movie S1. Snapshots of slip rate from the dynamic rupture of the Mw 7.8 Kahramanmaras earthquake.

Movie S2. The ratio of shear stress and normal stress during the triggering process. A ratio equal to $\boldsymbol{\mu_s}$ (0.4) indicates the position of the rupture front in the EAF.

References in the Supporting Information

Güvercin, S. E., Karabulut, H., Konca, A. Ö., Doğan, U., & Ergintav, S. (2022). Active seismotectonics of the East Anatolian Fault, *Geophysical Journal International*, *230*(1), 50-69, https://doi.org/10.1093/gji/ggac045.

Khalifa, A., Çakır, Z., Owen, L., & Kaya, Ş. (2018). Morphotectonic analysis of the East Anatolian Fault, Turkey, *Turkish Journal of Earth Sciences, 27*(2), 110-126, https://doi.org/10.3906/yer-1707-16.